

HELIOSEISMIC MAPPING OF THE MAGNETIC CANOPY IN THE SOLAR CHROMOSPHERE

W. FINSTERLE AND S. M. JEFFERIES¹

Maui Scientific Research Center, University of New Mexico, 590 Lipoa Parkway, Suite 262, Kihei, HI 96753; wfinsterle@spd.aas.org, stuartj@msrc.unm.edu

A. CACCIANI AND P. RAPEX

Dipartimento di Fisica, Università degli Studi di Roma “La Sapienza,” Piazzale Aldo Moro, 2, I-00185 Rome, Italy;
alessandro.cacciani@roma1.infn.it, paolo.rapex@fastwebnet.it

AND

S. W. MCINTOSH

Universities Space Research Association, Cooperative Program in Space Science, Seabrook, MD 2070; and Laboratory for Astronomy and Solar Physics,
NASA Goddard Space Flight Center, Mail Code 682.3, Greenbelt, MD 20772; scott@grace.nascom.nasa.gov

Received 2004 May 10; accepted 2004 August 11; published 2004 August 30

ABSTRACT

We determine the three-dimensional topography of the magnetic canopy in and around active regions by mapping the propagation behavior of high-frequency acoustic waves in the solar chromosphere.

Subject headings: Sun: chromosphere — Sun: helioseismology — Sun: magnetic fields

Over the past two decades our understanding of the solar interior has grown substantially through the use of various helioseismic methods such as sound speed and rotational inversions of measured p -mode frequencies, time-distance cross-correlation, and acoustic holography. Compared to the possibilities these methods provide for three-dimensional imaging of subsurface layers, the available tools to explore the outer solar atmosphere are still very basic. Classical helioseismic tools usually rely on the analysis of waves with frequencies below the acoustic cutoff frequency that are essentially trapped in the internal acoustic cavity of the Sun. These waves are largely evanescent in the outer atmosphere and carry little information on this region. The classical helioseismic tools therefore fail to constrain the plasma topology outside the acoustic cavity. The situation changes for waves with frequencies above the acoustic cutoff frequency: these waves propagate freely in the atmosphere. When they encounter a boundary across which there is a change in the dispersive characteristics of the medium, they are refracted and reflected (cf. geometric optics). Numerical simulations by Rosenthal et al. (2002), of wave propagation in a two-dimensional magnetoatmosphere, have shown that the region where the magnetic and gas pressures become comparable (i.e., $\beta = 8\pi p_g/B^2 \sim 1$, where p_g is the gas pressure and B is the magnetic field strength) provides such a boundary. Since the gas pressure drops off more rapidly with increasing height than does the magnetic pressure, then β decreases with increasing height regardless of the photospheric field strength. Thus the β -transition region (i.e., the $\beta \sim 1$ layer) partitions the atmosphere into contiguous volumes of high- β and low- β plasma (McIntosh et al. 2001; Rosenthal et al. 2002) and acts as a “magnetic canopy” for the waves (Bogdan et al. 2003). In quiet Sun this canopy is expected to vary in height between roughly 0.8 and 1.6 Mm above the base of the photosphere (Rosenthal et al. 2002). In active regions the canopy is lower, and in sunspots it can even dip below the photosphere. Here we use the phase lag of the Doppler signal in different layers in the photosphere and low chromosphere to determine at which height the transition from the pressure-dominated (high- β) to the magnetic-dominated (low- β) plasma occurs.

The analyses presented in this Letter are based on three-dimensional data cubes (heliographic longitude \times heliographic latitude \times time) of multiheight Doppler data from the Magneto Optical Filters at Two Heights (MOTH) experiment taken in 2003 January and a contemporaneous cube of Michelson Doppler Imager (MDI) data (Scherrer et al. 1995). The MOTH data consist of rapid (10 s sampling) simultaneous dopplergrams in the photosphere (K I, 769.9 nm) and low chromosphere (Na I D2, 589.0 nm) taken at the South Pole (Finsterle et al. 2004). MDI takes dopplergrams in the photospheric Ni I (676.8 nm) line. Simultaneous observations in several atmospheric layers allow us to determine the propagation behavior of acoustic waves between these layers. All dopplergrams were remapped onto a grid of heliographic longitude and latitude with the solar differential rotation removed before stacking them into data cubes.

We used the dual-height ($13^\circ \times 13^\circ \times 68$ hr) cubes of quiet Sun data taken by the MOTH experiment between 2003 January 17 and 20 to estimate the phase and group travel times for acoustic waves as a function of frequency. The time series in the corresponding pixel of the Na and K data cubes were first frequency-filtered using a Gaussian $G(\omega)$ of width $\delta\omega = 0.4$ mHz and then cross-correlated. The resulting cross-correlation functions of K and Na were then fitted by least squares using

$$y(t) = \frac{A^2\delta\omega}{\sqrt{8\pi}} \exp\left[-\frac{\delta\omega^2(t - T_g)^2}{8}\right] \cos[\omega(t - T_p)] \quad (1)$$

(Jefferies et al. 1997), with T_p , T_g , A , ω , and $\delta\omega$ as variables. We allowed the width $\delta\omega$ to vary, as the effective width of the filter depends on both the filter and the shape of the underlying spectrum. The fits for T_p and T_g are displayed in Figure 1 for a set of 12 different frequencies ranging from 2.7 to 7.9 mHz. As expected for acoustic waves, the observed frequency variation of T_p and T_g is well described by the simple dispersion relation

$$\omega^2 = c^2k^2 + \omega_0^2, \quad (2)$$

with ω_0 denoting the acoustic cutoff frequency and c and k the sound speed and wavenumber, respectively. From equation (2)

¹ Steward Observatory, University of Arizona, 933 North Cherry Avenue, Tucson, AZ 85721.

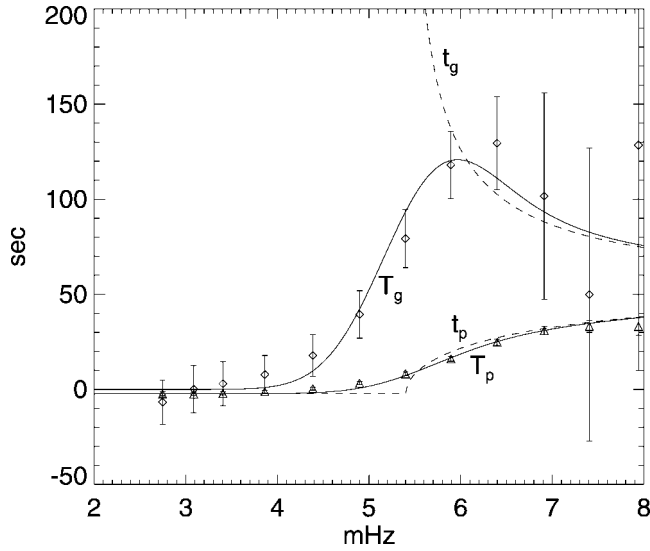


FIG. 1.—Group time (diamonds) and phase time (triangles) from a fit to the cross-correlation function of a 68 hr time series of Na and K dopplergrams in a $\sim(158 \text{ Mm} \times 158 \text{ Mm})$ area of quiet Sun using the function given by eq. (1). Overplotted are the theoretical group and phase times (t_g, t_p) according to eqs. (3) and (4) with $\omega_0 = 2\pi \times 5.4 \text{ mHz}$ and $\Delta z/c = 55 \text{ s}$ (dashed lines). The solid lines are the convolution of t_g and t_p with a Gaussian frequency filter of width 0.57 mHz, which is the effective width after the original frequency filter (0.4 mHz) was modulated by the shape of the spectrum. The error bars indicate the 1σ spread in the observed area.

the theoretical phase and group travel times for $\omega \geq \omega_0$ are given by

$$t_p = \frac{\Delta z}{\omega/k} = \frac{\Delta z}{c} \sqrt{1 - (\omega_0/\omega)^2} \quad (3)$$

and

$$t_g = \frac{\Delta z}{d\omega/dk} = \frac{\Delta z}{c} \frac{1}{\sqrt{1 - (\omega_0/\omega)^2}}, \quad (4)$$

where Δz is the height difference between the K and Na line-forming layers. The measured phase and group times $T_{p,g}$ are related to the theoretical values $t_{p,g}$ via convolution with the Gaussian frequency filter:

$$T_{p,g}(\omega) = (t_{p,g} * G)_\omega. \quad (5)$$

As shown in Figure 1, the curves for $t_{p,g} G(\omega)$ in the quiet Sun are in good agreement with the measured $T_{p,g}$ if we set the cutoff frequency $\omega_0 = 2\pi \times 5.4 \text{ mHz}$ and the wave travel time $t = \Delta z/c = 55 \text{ s}$. For convenience we use this result to determine the scaling factor:

$$R(\omega) = \frac{t_p(\omega)}{(t_p * G)_\omega}. \quad (6)$$

Together with equation (3), $R(\omega)$ allows us to estimate the wave travel time from the fit to T_p at a single frequency (i.e., without the need to perform a frequency scan), according to

$$t = \frac{\Delta z}{c} = \frac{t_p}{\sqrt{1 - (\omega_0/\omega)^2}} = \frac{R(\omega)T_p}{\sqrt{1 - (\omega_0/\omega)^2}}. \quad (7)$$

TABLE 1
QUIET-SUN WAVE TRAVEL TIMES BETWEEN THE
OBSERVING HEIGHTS SAMPLED BY Ni, K, AND Na
OBSERVATIONS

Line	K (s)	Na (s)
Ni	31 ± 5	90 ± 8
K	55 ± 4

NOTES.—Quiet-Sun wave travel times are estimated from 17.8 hr data cubes by determining the phase lags of 7 mHz waves (eq. [7]). The wave travel time between the K and Na layers agrees with the result obtained from fitting the frequency scan of the group time and phase time of 68 hr data cubes (Fig. 1).

Fitting T_p tends to be much more robust than fitting the group time T_g (compare error bars in Fig. 1). Estimating t from T_p alone thus allows us to use shorter time series without a significant loss in accuracy. Since R is independent of Δz we can also use equation (7) to estimate the wave travel times for the MOTH-MDI combined data sets. The results of such a combined analysis are shown in Figure 3 where we used ($40^\circ \times 40^\circ \times 17.8 \text{ hr}$) cubes of MOTH and MDI starting on 2003 January 20, 00:59 UT, which is the longest overlapping stretch of MOTH and MDI observations, to produce maps of the wave travel time between the Ni, K, and Na line formation layers. The MOTH and MDI images were coregistered by maximizing the cross-coherence of the p -mode signal in both data sets. For the travel time maps in Figure 3, a Gaussian frequency filter centered at 7 mHz of width 0.4 mHz was used. The resulting scaling factor for the phase time is $R \approx 1.1$ (eq. [6]).

In quiet-Sun areas² the wave travel times have constant values given in Table 1. In active regions the wave travel time gradually decreases with increasing photospheric field strength and even vanishes in some areas where the magnetic field is the strongest. In these areas the 7 mHz waves behave as though they are evanescent. This can be explained by a simple model in which the $\beta \sim 1$ magnetic canopy reflects acoustic waves. Here, when the upper observing layer is in a low- β region (i.e., above the $\beta \sim 1$ canopy), we only measure the evanescent tails of the reflected waves (Fig. 2). Since the phase of an evanescent wave does not change with height, t in equation (7) represents

² Regarding wave propagation, we define “quiet Sun” as areas where the waves do not penetrate the low- β plasma. We chose areas where $\beta > 20$ at the Na level.

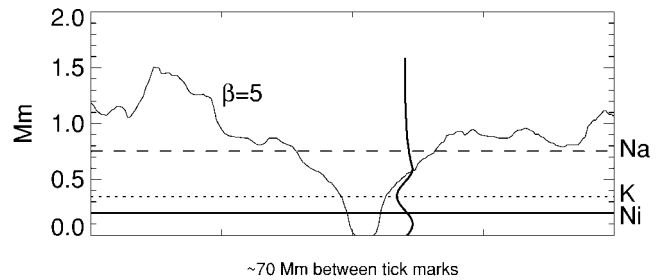


FIG. 2.—Vertical cut through the $\beta = 5$ surface above a sunspot with the horizontal lines indicating the formation heights for the Ni (solid line), K (dotted line), and Na (dashed line) lines. The position of the cut is marked by the red line in Fig. 3d. Our reflection model is visualized by a schematic wave train (wavelength not to scale). The upward traveling wave is reflected at the $\beta = 5$ surface, and only its evanescent tail reaches the Na layer. For simplicity the reflected wave is not shown. Fig. 8 of Rosenthal et al. (2002) suggests that the reflected wave travels downward at an angle away from the sunspot.

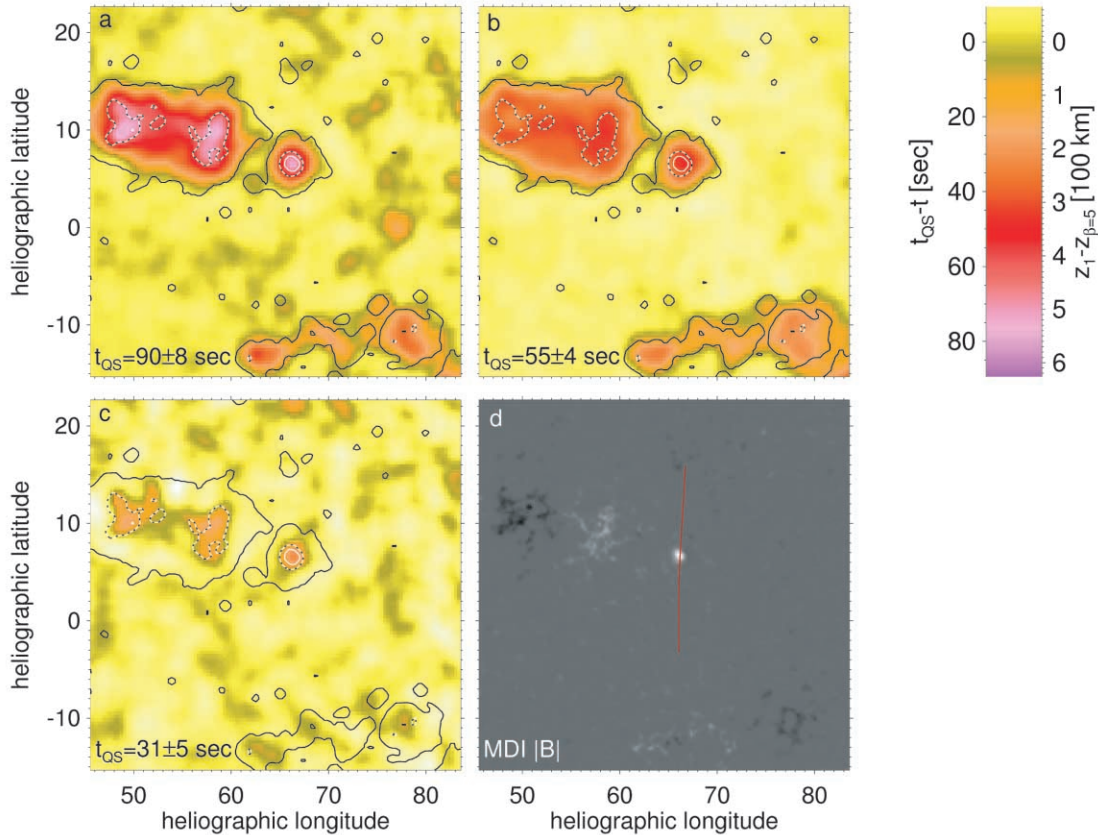


FIG. 3.—Maps of travel time for 7 mHz waves between the (a) Ni and Na, (b) K and Na, and (c) Ni and K layers and (d) the contemporaneous MDI magnetogram. Overlaid on the travel time maps are the $\beta = 5$ contours at 200 ± 50 km (white), 420 ± 50 km (black-white), and 800 ± 50 km (black) above the base of the photosphere ($\tau_{500} = 1$). Assuming the Ni line to be formed at 200 km (Georgobiani et al. 2000), the black and black-white contours agree with the formation heights of Na and K lines calculated from the quiet-Sun wave travel time t_{QS} (Table 1) with a sound speed of $c = 7$ km s $^{-1}$. Under the same assumption the color scale can be interpreted in terms of canopy height with respect to the upper observing level (z_1). The reflection model predicts panels a and b to be equivalent except inside the black-white contours, where panel a shows the canopy height between the Ni and K layers. This is consistent with the Ni-K travel time map of panel c, which also scans the canopy between the Ni and K layers. The red line in panel d marks the location of the vertical cut shown in Fig. 2. Note that to reduce high spatial frequency noise, the maps have been smoothed using a 5×5 pixel boxcar function.

the travel time between the lower observing layer and the $\beta \sim 1$ canopy if this surface crosses between the two observing heights, or the travel time between the heights otherwise.

To test the validity of the above hypothesis, we have estimated the height of the magnetic canopy for our observations using a potential field extrapolation of the MDI magnetogram taken at the half-time point of the 17.8 hr data cube, and a standard VAL C (Vernazza et al. 1981) model atmosphere (McIntosh et al. 2001). We emphasize that using these methods to compute the magnetic and gas pressures only provides a *quantitative* description of how the $\beta \sim 1$ layer behaves throughout the atmosphere. First, it is known that even in the quiet Sun the magnetic field configuration is significantly non-potential (Woodard & Chae 1999), and second, the VAL C model is a static model that is incapable of reproducing all the effects of a highly dynamic atmosphere. In addition, the effective height of wave reflection will have some dependence on the frequencies of the waves (Rosenthal et al. 2002) admitted into the analysis by our filter. With these considerations in mind, we have chosen to use the $\beta = 5$ surface as our proxy to the $\beta \sim 1$ region. This choice provided the best agreement between the measured quiet-Sun travel time data and the expected height of formation of our observing lines (Ni, K, and Na) in the VAL C model. However, we note that the height difference between

the $\beta = 1$ and 5 surfaces in the active regions shown in the magnetogram in Figure 3d is of the order of 25–50 km depending on the base field strength. Figures 3a, 3b, and 3c show maps of the wave travel time between two heights z_0, z_1 , where $z_0 \in \{z_{Ni}, z_K\}$, $z_1 \in \{z_K, z_{Na}\}$, and $z_1 > z_0$, overlaid with the corresponding $\beta = 5$ contours. All the maps demonstrate the following: outside the $\beta = 5$ contours at the z_1 level, the maps are consistent with quiet-Sun wave travel time, while inside these contours the wave travel time gradually decreases. Inside the $\beta = 5$ contours at the z_0 level the travel time maps are consistent with a vanishing wave travel time, i.e., evanescent waves. Since the maps in Figures 3a and 3b share the same upper observing layer, the wave reflection hypothesis predicts that they should only be different from each other inside the $\beta = 5$ contours at the K level (black-white contours). Inside these contours the magnetic canopy is below the K layer, and therefore the K-Na maps do not reveal the height of the canopy in this region, while the Ni-Na map scans the height of the canopy down to the Ni level. A consistent image of the canopy height between the Ni and K layers is given in the Ni-K travel time map of Figure 3c. Under the assumption of a constant sound speed, the maps of wave travel time with respect to the quiet Sun in Figure 3 can also be interpreted as maps of the canopy height with respect to the upper observing layer.

The determination of the height of the $\beta \sim 1$ canopy offers a potential way to constrain magnetic field extrapolations and solar atmospheric models by relating gas pressure to magnetic pressure. In particular, our results suggest the possibility to estimate the magnetic field strength using magnetically *non-sensitive* lines. Since there are few chromospheric lines that are suitable for measuring magnetograms, this is a considerable advantage. Furthermore, as Bogdan et al. (2003) pointed out, knowing whether the spectral line is formed in the high- β or low- β plasma is essential for deciphering the complex observational signal in low- β regions. Our results show that observing high-frequency waves at two or more heights can help determine the location of the canopy.

Time closure for the mutual wave travel times between the three observing layers Na, K, and Ni is observed, within the measured uncertainties, in both the high- β and the low- β regions (Table 1; Fig. 3). We note that an additional uncertainty in the results arises from systematic phase lags between the Doppler signals in each line. For K and Na this systematic phase lag shows an east-west dependence, due to velocity contamination in the intensity signal used to normalize the dopplergrams (cf. Finsterle et al. 2004), resulting in an east-west gradient of ~ 0.1 s per heliographic degree on the travel time maps. This east-west gradient has been removed from the maps in Figure 3. The Ni-K and Ni-Na wave travel time maps (Figs. 3a and 3c) are substantially noisier than the K-Na map of Figure 3b because the 60 s cadence observations of the Ni line had to be oversampled in order to detect subminute lags. The uncertainty

in the height of the $\beta = 5$ extrapolation, estimated by Monte Carlo variants of the base field, is of the order of ± 50 km.

In summary, we have found that wave travel time maps calculated from our observations at three heights in the atmosphere show time closure in active regions as well as in the quiet Sun. The observed features in these maps are consistent with wave reflection from an intermediate layer. We propose that the $\beta \sim 1$ magnetic canopy provides this layer, a suggestion that is supported by two-dimensional numerical simulations of wave propagation in a magnetoatmosphere (Rosenthal et al. 2002). In this scenario, contours of $\beta \sim 1$ should agree with the travel time contours: we show very good agreement with the $\beta = 5$ contours. This suggests that we are measuring the location of the magnetic canopy throughout the three-dimensional volume between the lower and upper observing heights. We note that the presence of a reflecting layer in the chromosphere could explain the chromospheric resonances reported by Worrall (2002).

This work was funded by award OPP-0087541 from the National Science Foundation and by ENEA-Progetto Antaride. We thank Stanford University for supporting the work on the *SOHO/MDI-MOTH* joint data sets. *SOHO* is a project of international cooperation between ESA and NASA. We also thank D. Longcope, T. Bogdan, C. Lindsey, and D. Braun for discussions related to this work and the referee for critical comments that have helped improve this manuscript. S. W. M. is partly supported by the National Aeronautics and Space Administration under grant NNG04GG34G issued under the Sun-Earth Connection Guest Investigator Program.

REFERENCES

- Bogdan, T. J., et al. 2003, *ApJ*, 599, 626
 Finsterle, W., Jefferies, S. M., Cacciani, A., Rapex, P., Giebink, C., Knox, A., & DiMartino, V. 2004, *Sol. Phys.*, 220, 317
 Georgobiani, D., Kosovichev, A. G., Nigam, R., Nordlund, Å., & Stein, R. F. 2000, *ApJ*, 530, L139
 Jefferies, S. M., Osaki, Y., Shibahashi, H., Harvey, J. W., D'Silva, S., & Duvall, T. L., Jr. 1997, *ApJ*, 485, L49
 McIntosh, S. W., et al. 2001, *ApJ*, 548, L237
 Rosenthal, C. S., et al. 2002, *ApJ*, 564, 508
 Scherrer, P. H., et al. 1995, *Sol. Phys.*, 162, 129
 Vernazza, J. E., Avrett, E. H., & Loeser, R. 1981, *ApJS*, 45, 635
 Woodard, M. F., & Chae, J. 1999, *Sol. Phys.*, 184, 239
 Worrall, G. 2002, *MNRAS*, 335, 628